Total neutron scattering investigation of the structure of a cobalt gallium oxide spinel prepared by solvothermal oxidation of gallium metal

Total neutron scattering investigation of the structure of a cobalt gallium oxide spinel prepared by solvothermal oxidation of gallium metal

Helen Y Playford[1,2]**, Alex C Hannon**[3]**, Matthew G Tucker**[3]**, Martin R Lees**[2] **and Richard I Walton**[1]

[1] Department of Chemistry, University of Warwick, Coventry, West Midlands, CV4 7AL, UK
[2] Department of Physics, University of Warwick, Coventry, West Midlands, CV4 7AL, UK
[3] ISIS Facility, Rutherford Appleton Laboratory, Didcot, Oxfordshire, UK

E-mail: r.i.walton@warwick.ac.uk

Abstract
A new solvothermal synthesis route to mixed-metal gallium oxides with the spinel structure has been developed for ternary oxides of ideal composition $Ga_{3-x}M_xO_{4-y}$ (M = Co, Zn, Ni). The structure of the novel cobalt gallate produced in this manner, $Ga_{1.767(8)}Co_{0.973(8)}O_{3.752(8)}$, has been determined from total neutron scattering to be a partially defective spinel with mixed-valent cobalt (approximately 25% Co^{3+} and 75% Co^{2+}) and with vacancies on approximately 6% of oxygen sites. Pair distribution function (PDF) analysis reveals significant local deviations from the average cubic structure, which are attributed to the conflicting coordination preferences of the Co^{2+} (potential Jahn–Teller distortion) and Ga^{3+} (Ga off-centring). Reverse Monte Carlo (RMC) modelling supports this conclusion since different metal–oxygen bond-distance distributions are found for the two cations in the refined configuration. An investigation of magnetic properties shows evidence of short-range magnetic order and spin-glass-like behaviour, consistent with the structural disorder of the material.

[S] Online supplementary data available from stacks.iop.org/JPhysCM/25/454212/mmedia

1. Introduction

Mixed-metal oxides with the spinel structure have been extensively investigated as important functional materials for many years. It is the combination of ferromagnetism and electrical conductivity that led to initial industrial interest in spinels, particularly the ferrites, for applications in electronics and magnetic data storage [1]. This focus continues to this day, with new interests in transparent conducting oxides [2], lithium-containing spinels for battery materials [3], and many potential applications in catalysis [4, 5] and photocatalysis [6].

The vast range of different properties exhibited by spinel oxides can be attributed to the flexibility and inherent disorder of the structure. Consisting of a near-perfect cubic close packed array of oxide ions with cations residing in fractions of the octahedral and tetrahedral interstices, the spinel structure can accommodate many different numbers and types of cation. It is common to use the empirical formula AB_2O_4, where A is a divalent cation and B is a trivalent cation, to describe an oxide spinel. A 'normal' spinel is one in which the trivalent (B) cations occupy the octahedral sites, and the divalent (A) cations occupy the tetrahedral sites, however, in any given material, the distribution of A and B cations is often variable, depending on the synthesis conditions, and may also be affected by temperature and pressure. An inversion parameter, x, may be defined as the proportion of divalent (A) cations occupying the octahedral sites, as per the formula $^{IV}(A_{1-x}B_x)^{VI}[A_xB_{2-x}]O_4$ [7, 8]. As well as cation disorder, it is common for spinel oxides to adopt defective structures where some of the cation

sites are vacant, such as in maghemite, γ-Fe_2O_3 [9], or for extra cation sites to be occupied in addition to the usual two, examples of which are found in γ-Al_2O_3 [10], the lithium-rich spinel $Li_{1+x}Mn_{2-x}O_4$ [11], and naturally occurring $Mg_{0.04}Fe_{2.96}O_4$ [12].

A full structural description of a disordered material must include information about the local structure, as well as the average structure obtained from crystallographic methods [13, 14]. This is particularly important for nano-scale materials, in which the short length scale of any structural coherence may limit or remove altogether the applicability of conventional crystallography. The likelihood of significant differences in both structure and properties when moving from the bulk to the nano-scale necessitates the detailed characterization of these materials.

Local structure and disorder in spinels have often been probed using spectroscopic techniques such as x-ray absorption spectroscopy, nuclear magnetic resonance (NMR), and Raman and Mössbauer spectroscopy. For example, while bulk zinc ferrite, $ZnFe_2O_4$, is a normal spinel, an extended x-ray absorption fine structure (EXAFS) study revealed a correlation between particle size and an increasing degree of inversion, and that nanoparticles with either Zn- or Fe-rich compositions exhibited extremely disordered cation distributions with Zn and Fe able to swap readily between sites [15]. Solid-state ^{27}Al NMR was used to examine a series of synthetic $MgAl_2O_4$ nanoparticles and found evidence for 3- and 5-coordinate aluminum sites in the smallest particles, attributed to surface defects, and for a second, distorted, 6-coordinate environment in the larger particles, which was related to the degree of inversion [16]. Evidence for a core–shell structure was obtained from NMR and Raman spectroscopy of mechanochemically synthesized $SnZn_2O_4$ nanoparticles, by comparison with spectra from the bulk material [17]. While the core region was ordered and had an inverse cation arrangement (as in the bulk) the surface region exhibited highly disordered polyhedra and random cation distribution. These spectroscopic techniques, while powerful, offer little insight into the relationship between local distortions and the structure as a whole.

The use of x-ray and/or neutron total scattering techniques, wherein both the Bragg and diffuse scattering are analysed (rather than just the Bragg scattering as is the case in conventional crystallographic analysis) reveals structural information on a range of length scales. In the case of nano-scale or disordered materials, it is common to examine local structure via analysis of the atomic pair distribution functions (PDFs) obtained by Fourier transform of the total scattering data. For example, in the case of the spinel $CuMn_2O_4$, which adopts a tetragonal structure due to Jahn–Teller distortion of both cation sites, the structure obtained from Rietveld refinement reproduced the measured PDF well at longer distances, whereas reverse Monte Carlo modelling revealed that the material exhibits complex short-range disorder, with evidence that a fraction of both Cu^{2+} and Mn^{3+} cations disproportionate in order to reduce the Jahn–Teller effect on a local scale [18].

This paper is concerned with gallate spinels where gallium and a transition-metal cation occupy the sites of the spinel structure. An early report by Navrotsky *et al* described a number of AGa_2O_4 materials for A = Mg, Co, Ni, Cu, Zn or Cd [19], and subsequently, gallate spinels have been investigated as potential transparent conductors [20, 21], luminescent materials [22–24], gas sensing materials [25], and photocatalysts [26, 27]. Cobalt gallate spinels have been rather less studied than those of other metals. $CoGa_2O_4$ has generally been classified as a partially inverse spinel, though the exact value of the inversion parameter has not been consistently reported [28–30]. $CoGa_2O_4$ has also been reported to exhibit spin-glass behaviour at low temperatures due to the distribution of Co^{2+} ions across both cation sites [29, 31]. The cation arrangement in gallate spinels is potentially extremely flexible due to Ga^{3+} not exhibiting a strong preference for tetrahedral or octahedral coordination: in the thermodynamically stable polymorph β-Ga_2O_3, gallium occupies sites of both geometries in equal proportions [32].

In this paper we describe a full structural investigation of a new cobalt gallate spinel prepared using a mild solvothermal synthesis method and compare its structure to related materials already reported in the literature. This type of mild synthetic approach is of particular interest for functional materials because it can allow control of crystallite size and shape, for example to produce fine powders which may be easily processed for real applications, or to produce nanosized particles with unusual electronic and magnetic properties [33, 34]. Additionally, changing synthesis temperature may affect the cation distribution in spinels, as has been observed for $CoGa_xAl_{2-x}O_4$ solid solutions [35]. This means that, for a given composition, spinels produced by solvothermal or high-temperature synthesis may be considered to be different polymorphs with distinct sets of properties. Given the various possibilities of disorder in the spinel structure described above, we have used pair distribution function analysis to build up a comprehensive structural model of the cobalt gallate spinel and we have related this to the average structure determined by Rietveld analysis and measurements of magnetic properties. Neutron scattering was the method of choice for this study; the high Q-range made accessible by the time-of-flight method at a spallation source offers high real-space resolution for accurate modelling, and the neutron scattering lengths of Co, Ga and O differ sufficiently (Co = 2.49 fm, Ga = 7.288 fm, O = 5.803 fm [36]) for them all to be distinguished by this method (which is the not case for x-ray scattering since the atomic numbers of the two metals differ by only four).

2. Experimental details

2.1. Synthesis

We recently reported the synthesis of spinel-structured γ-Ga_2O_3 via the solvothermal oxidation of gallium metal in an aminoalcohol solvent [37], based on the work of Kim *et al* [38], but optimized for lower temperatures. We now report the extension of this technique to the synthesis of mixed oxides via the addition of transition-metal salts to the reaction mixture. In this manner, mixed spinels of ideal

composition $M_xGa_{3-x}O_4$ with M = Zn, Ni and Co have been synthesized. In a typical synthesis, 0.1 g (1.4 mM) of metallic gallium (Aldrich 99.99%) and an appropriate amount of either $ZnCl_2$, $Ni(NO_3)_2 \cdot 6H_2O$ or $Co(NO_3)_2 \cdot 6H_2O$ (0.7, 1.4 or 2.8 mM) were added to 5 ml of 2-aminoethanol (Aldrich $\geq$ 99.0%) or diethanolamine (Aldrich $\geq$ 98.5%) in a $\sim$20 ml Teflon® autoclave liner and heated in a water bath at $\sim$70 °C for 10–15 min. The reaction mixtures were then sealed in a stainless-steel autoclave and heated in a fan oven at 240 °C for six days. Interestingly, in all cases some reduction of the M^{2+} salts had occurred, as evidenced by the presence of metallic Zn, Ni and Co in the products. In the case of the cobalt-containing spinel this impurity was easily removed via dispersion in methanol followed by filtration through a funnel lined with small rare-earth magnets. The examination of the Zn and Ni gallate spinels using powder x-ray diffraction revealed that their lattice parameters were in good agreement with those previously published for materials of the same composition, and since both Zn and Ni are likely only to adopt the +2 oxidation state and they exhibit strong preference for tetrahedral and octahedral coordination, respectively, it was considered that the potential for disorder in these structures was small; the focus of this paper is therefore the novel cobalt gallate.

2.2. General characterization

Transmission electron microscopy (TEM) images were collected using a JEOL 2000FX instrument operating at 200 kV, and energy dispersive x-ray (EDX) spectra were measured with an attached EDAX Genesis system. Prior to measurement, samples were ultrasonically dispersed in ethanol and deposited onto 3 mm lacy carbon grids.

Magnetometry was performed using a Quantum Designs MPMS-5S SQUID magnetometer. Measurements of the dc magnetization were made in magnetic fields of up to 50 kOe in the temperature range 2–300 K. Measurements of the ac susceptibility versus temperature were made at frequencies of 0.05–30 Hz with an ac driving field of 3 Oe in dc bias fields of up to 10 kOe.

Density measurements were performed using a Micromeritics AccuPyc 1340 gas pycnometer. Powder samples were loaded into a cell of volume 1 cm^3 ($\sim$2/3 fill) and purged under a flow of helium gas for 1 h prior to measurement.

2.3. Neutron scattering

Total neutron scattering experiments were carried out using the GEneral Materials diffractometer (GEM) at ISIS, the UK spallation neutron source [39]. Samples were loaded into cylindrical vanadium foil cans with inner diameter 0.5 cm and wall thickness 0.0025 cm, and data were collected for 4 h to ensure good statistical quality. Data were also collected from an empty can, the empty instrument and a 0.834 cm diameter vanadium rod for normalization purposes. The data were reduced and corrected using the GudrunN [40, 41] and ATLAS [42] software to obtain the distinct scattering, $i(Q)$, the result of subtracting calculated self-scattering from the measured total scattering, as in equation (1), where Q is the magnitude of the scattering vector.

$$i(Q) = I(Q) - I^S(Q). \tag{1}$$

Once corrected for the effect of the incoherent scattering from hydrogen (see supporting information available at stacks. iop.org/JPhysCM/25/454212/mmedia), the $i(Q)$ was Fourier transformed to obtain the differential correlation function, $D(r)$ (equation (2)).

$$D(r) = \frac{2}{\pi} \int_0^{Q_{max}} Qi(Q)\, M(Q)\, \sin\, rQ\, \mathrm{d}Q \tag{2}$$

where $Q_{max} = 32$ Å^{-1} and $M(Q)$ is the Lorch modification function, used to reduce the termination ripples due to the finite value of Q_{max} [43]. The function $D(r)$ is hereafter referred to as the pair distribution function (PDF). The program GSAS within EXPGUI [44, 45] was used for Rietveld refinement of the corrected neutron diffraction data and the program PDFgui was used for PDF analysis [46]. The program RMCProfile was used for reverse Monte Carlo modelling [47]. Datasets used for RMC refinements were the aforementioned $i(Q)$ and the correlation function $G(r)$ (equation (3)).

$$G(r) = \frac{D(r)}{4\pi r \rho_0}. \tag{3}$$

Several features in the low-r region of the latter were found to shift significantly on adjusting the Q-range of the Fourier transform and were thus determined to be nonphysical, thus the ranges 0–1.68 Å and 2.24–2.54 Å were excluded from the RMC fit.

3. Results and discussion

3.1. General characterization

Transmission electron microscopy images of the cobalt gallate spinel are shown in figure 1. The sample consists of highly crystalline nanoparticles, 20–40 nm in diameter, and analysis of EDX spectra from several crystallites reveals a Co:Ga ratio of 1:1.94. The result of Co K-edge XANES spectroscopy (see supporting information available at stacks.iop.org/JPhysCM/25/454212/mmedia) is consistent with the majority of Co being present in the +2 oxidation state, and the small magnitude of the pre-edge feature suggests that little Co is situated on the tetrahedral site of the spinel lattice, as this feature is attributed to a 1s–3d transition, which is forbidden for ions in centrosymmetric environments.

Thermogravimetric analysis revealed two small mass losses at 100–400 °C, which were attributed to the loss of small amounts of surface water and residual organic species from the synthesis. No evidence for oxidation or any other phase transition was found up to 1000 °C. This was supported by *in situ* powder x-ray diffraction, wherein the sample was shown to be stable over the temperature range studied (30–900 °C) (see supporting information available at stacks. iop.org/JPhysCM/25/454212/mmedia).
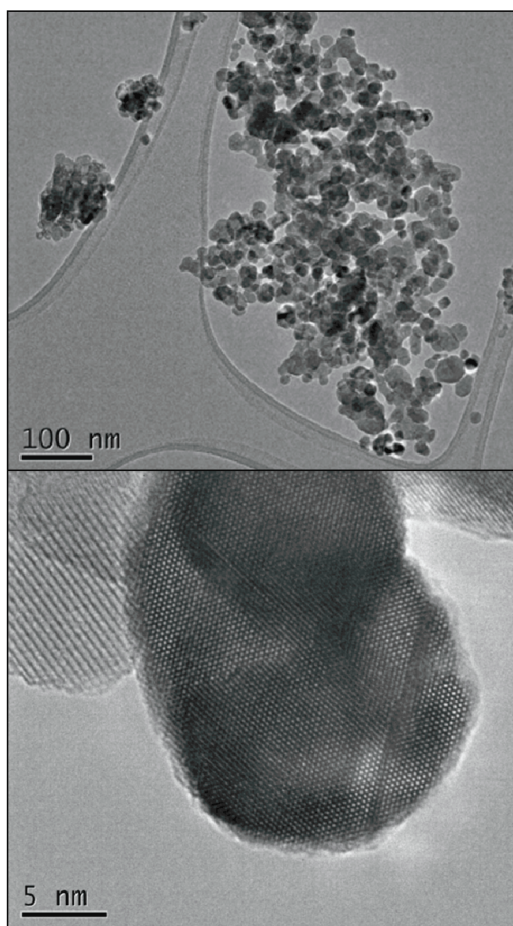
Figure 1. TEM images of the cobalt gallate spinel at two magnifications.

Table 1. Crystal parameters of the $CoGa_2O_4$ starting model for the cobalt gallate spinel. Space group $Fd\bar{3}m$, $a = 8.3281$ Å [28].

Site	Atom	x	y	z	Occupancy
8a	Ga	0.125	0.125	0.125	0.425
	Co	0.125	0.125	0.125	0.575
16d	Ga	0.5	0.5	0.5	0.288
	Co	0.5	0.5	0.5	0.712
32e	O	0.25842	0.25842	0.25842	1.00

3.2. Neutron scattering

3.2.1. Rietveld refinement. The starting point for Rietveld refinement of neutron diffraction data was a stoichiometric
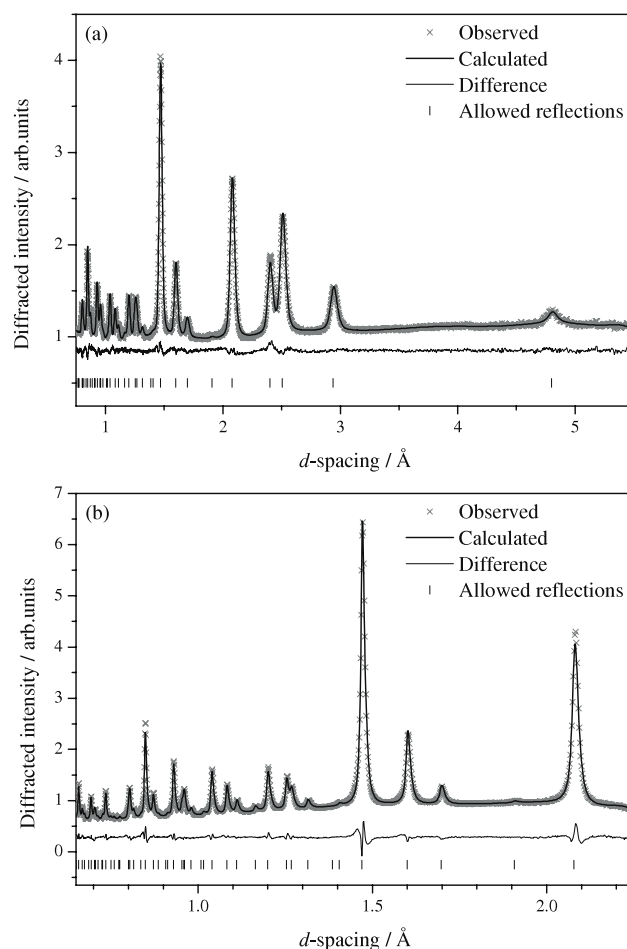

Figure 2. Result of Rietveld refinement for solvothermal cobalt gallate using the stoichiometric $CoGa_2O_4$ as a starting model. Refined simultaneously were (a) data from GEM bank 3 (mean scattering angle 34.9°) and (b) data from GEM bank 5 (mean scattering angle 91.3°). $Rp = 1.49\%$, $wRp = 2.38\%$.

$CoGa_2O_4$ model, as determined by Nakatsuka *et al* [28] from a single crystal sample of the material (table 1). The inversion parameter of the starting model was 0.575, indicating a distribution of cations across both tetrahedral and octahedral sites as shown by the refined formula: $^{IV}(Co_{0.425}Ga_{0.575})^{VI}[Co_{0.2875}Ga_{0.7125}]_2O_4$. The results of Rietveld refinement of the solvothermal $CoGa_2O_4$ are shown in figure 2 and table 2. A constraint was initially applied to the occupancies of the cation sites to maintain 100% occupancy on both sites. When this constraint was lifted the occupancies

Table 2. Refined crystal parameters for $Co_{1.106(8)}Ga_{1.893(8)}O_{3.95}$ from Rietveld analysis. Space group $Fd\bar{3}m$, $a = 8.31393(8)$ Å. Measured density $= 5.437$ g cm^{-3}, calculated density $= 6.019$ g cm^{-3}.

Site	Atom	x	y	z	U_{iso} (Å^2)	Occupancy
8a	Ga	0.125	0.125	0.125	0.0069(2)	0.796(4)
	Co	0.125	0.125	0.125	0.0069(2)	0.204(4)
16d	Ga	0.5	0.5	0.5	0.0077(2)	0.549(3)
	Co	0.5	0.5	0.5	0.0077(2)	0.451(3)
32e	O	0.25628(6)	0.25628(6)	0.25628(6)	0.0065(2)	0.987[a]

[a] Note that the occupancy of the oxygen site was not refined.

Table 3. Crystal parameters for $Co_{0.973(8)}Ga_{1.767(8)}O_{3.752(8)}$. Space group $Fd\bar{3}m$, $a = 8.312\,82(9)$ Å. Measured density = 5.437 g cm^{-3}, calculated density = 5.563 g cm^{-3}.

Site	Atom	x	y	z	U_{iso} (Å^2)	Occupancy
8a	Ga	0.125	0.125	0.125	0.0058(1)	0.745(4)
	Co	0.125	0.125	0.125	0.0058(1)	0.175(4)
16d	Ga	0.5	0.5	0.5	0.0058(1)	0.511(3)
	Co	0.5	0.5	0.5	0.0058(1)	0.399(3)
32e	O	0.25641(6)	0.25641(6)	0.25641(6)	0.0064(1)	0.938(2)

refined to unphysically large values and the *wR*p decreased only slightly, from 2.38% to 2.37%, and therefore this was not considered to be a significant result.

It can be seen from these results that solvothermal cobalt gallate in this model is largely inverse ($x = 0.796$) and that it appears to be slightly Co rich (Co:Ga ratio = 1:1.73). For this reason, a small number (1.3%) of oxygen vacancies were introduced to maintain the charge balance. A Fourier difference map was calculated to determine whether any cations were situated on non-spinel sites, as was found to be the case for γ-Ga_2O_3 [37], but none was identified in this case. It should be noted also that arbitrarily placing small amounts of either Ga or Co on the non-spinel sites did not improve the fit.

The significant discrepancy between the measured and calculated density (as shown in table 2) suggests that the solvothermal cobalt gallate would be better described by a model with lower density. Rietveld refinements using models based on the defect spinel structure of γ-Ga_2O_3 were not successful as the refined structures produced were extremely oxygen deficient (14% of oxygen sites vacant, a level of defects which has not been reported previously for a spinel and is unlikely to be stable), and the calculated densities extremely low.

In order to obtain a model consistent with the experimental observations of composition and density without excessive oxygen deficiency, it was necessary to introduce a small proportion of Co^{3+} rather than basing the model solely on Co^{2+}. The results of Rietveld refinement using this model are shown in figure 3 and table 3.

The density of this model gives a much closer match to the experimentally determined value. This model can be thought of as a partially defective model as it contains ~22 cations per unit cell, rather than the 24 in stoichiometric spinels or the $21\frac{1}{3}$ in defect spinels. The refined composition of $Co_{0.973(8)}Ga_{1.767(8)}O_{3.752(8)}$ indicates that 6.2% of the oxygen sites are vacant, an amount which is reasonable based on previous literature on oxygen-deficient spinels, such as a $LiMn_2O_{4-\delta}$ material found to have ~7% oxygen vacancies [48]. Charge balance requires that approximately 25% of the Co is in the +3 oxidation state, giving an average Co oxidation state of +2.26. This is not inconsistent with the Co K-edge XANES (see supporting information available at stacks.iop.org/JPhysCM/25/454212/mmedia), for which the spectrum of the cobalt gallate spinel was similar, but not identical, to the spectrum from the Co(II) standard. It may also be observed that the edge 'width' of the cobalt gallate is wider than that of the Co(II) standard but narrower than
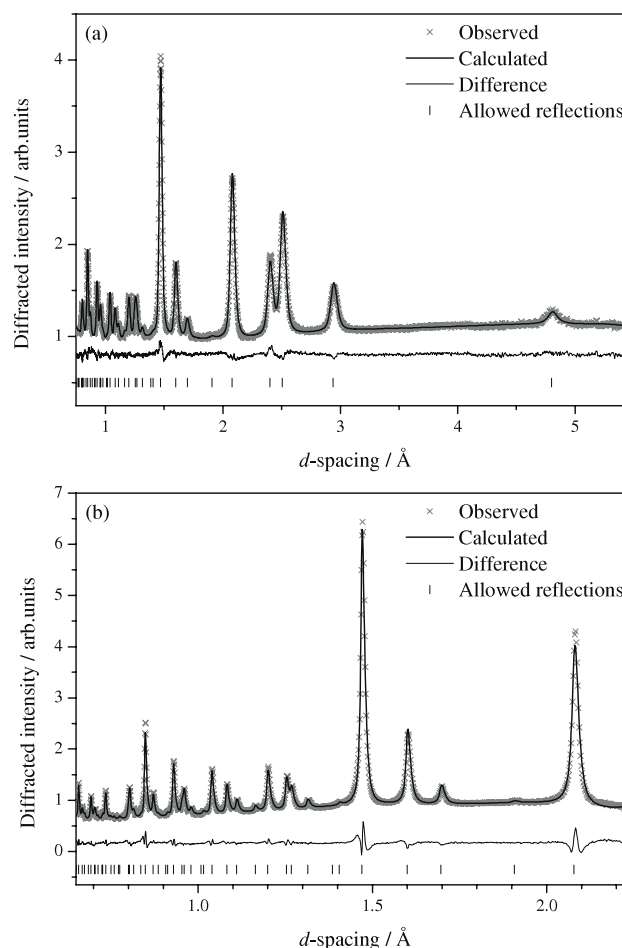

Figure 3. Result of Rietveld refinement for solvothermal cobalt gallate using the partially defective, mixed valence model, (a) data from GEM bank 3 (mean scattering angle 34.9°) and (b) data from GEM bank 5 (mean scattering angle 91.3°). Rp = 1.71%, wRp = 2.54%.

the mixed valent Co(II)/Co(III) standard—which is consistent with a degree of mixed valency in the spinel material [49].

3.2.2. Pair distribution function analysis. The arbitrary scale factor present in the Rietveld refinements discussed above prevents a meaningful differentiation between the two models being made, other than via comparison with an externally measured density. Conversely, the pair distribution function (PDF) obtained from the normalized total neutron scattering data allows direct comparison of the different models by means of the low-r slope of the data, $T^0(r)$, which is related
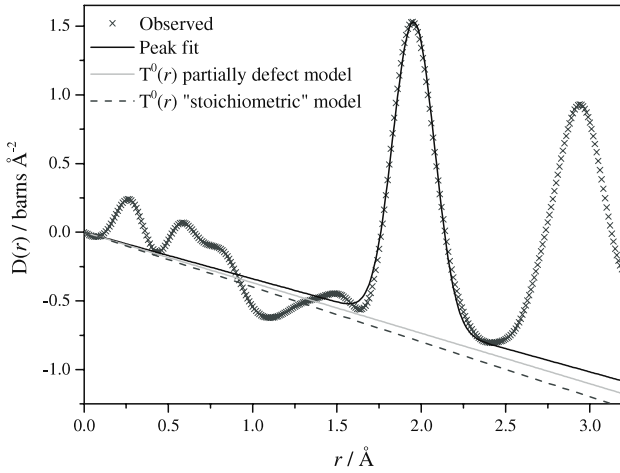
Figure 4. The measured PDF of the cobalt gallate spinel overlaid with the result of fitting the first peak, and the calculated $T^0(r)$ slopes for the two models.

to sample density and composition as per equation (3), where ρ = density, c_i = concentration of the ith atom and $\overline{b}_i$ = coherent neutron scattering length of the ith atom.

$$T^0(r) = 4\pi\rho_0 r \left(\sum_i c_i \overline{b}_i \right)^2. \qquad (4)$$

This comparison is shown in figure 4, and in this way it is clear that the partially defective model is the more appropriate.

The result of PDF analysis using this model is shown in figure 5. The fit shown was obtained after refining only the thermal parameters (supporting information available at stacks.iop.org/JPhysCM/25/454212/mmedia), and no further improvement was found to be possible through refinement within the parameters of the cubic spinel model.

However, on closer inspection of the low-r region of the fit, it can be seen that the Ga–O and Co–O correlations responsible for the first PDF peak are not adequately described by this model. This was also found to be the case for

γ-Ga$_2$O$_3$ and was attributed to a local distortion of the GaO$_6$ octahedra in which the Ga atoms are shifted closer to one face of the octahedron, resulting in three shorter and three longer Ga–O bonds [37]. In that case a model in non-centrosymmetric space group $F\overline{4}3m$ provided a suitable description of the anomaly; however the complete lack of any evidence for average symmetry lowering in the diffraction data highlighted the importance of using PDF analysis to investigate complex disordered materials. In the case of cobalt gallate, the added complexity of the mixed occupancy of the cation sites, with Co^{2+} likely to exhibit a Jahn–Teller type distortion and Ga^{3+} likely to exhibit the aforementioned off-centring, is likely to render any attempt at finding a local structure 'crystallographic' model, with the associated statistical distribution of cations, meaningless.

3.2.3. Reverse Monte Carlo (RMC). RMC modelling was undertaken to provide further insight into the structure of the material while avoiding the bias inherent in the crystal structure based analysis approaches. A $6 \times 6 \times 6$ supercell based on the Rietveld-derived model was generated, with the relevant proportions of Ga, Co and vacancies (Va) distributed randomly across the two cation sites. The two cation sites were defined separately such that the proportion of occupied octahedral and tetrahedral sites in the RMC configuration remained consistent with that in the average structural model. To allow for the possibility of non-random distribution of the cations (i.e. the potential for clustering or other short-to-medium-range ordering of Ga and Co) the various pairs (Ga–Co, Ga–Va and Co–Va) on each of the sites were allowed in turn to swap positions, with swap moves occurring at 30–40% of the probability of translational moves. The results from this refinement are shown in figure 6.

The RMC fits are consistent with the Rietveld and PDF analysis results: the mid-to-long-range order of the cobalt gallate material is well represented by a partially defective cubic spinel model. As can be seen from the collapsed unit cell (supporting information available at stacks.iop.org/JPhysCM/25/454212/mmedia), the atoms in the RMC configuration do
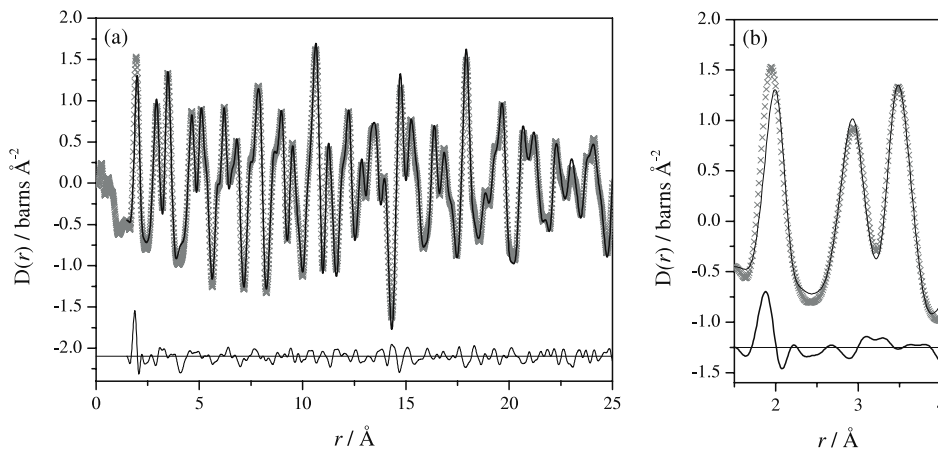

Figure 5. (a) The result of PDF analysis of the cobalt gallate spinel using the partially defective model. $wRp = 13.3\%$. (b) Close-up view of the low-r region of the fit, emphasizing the discrepancy in the shape and position of the first peak.
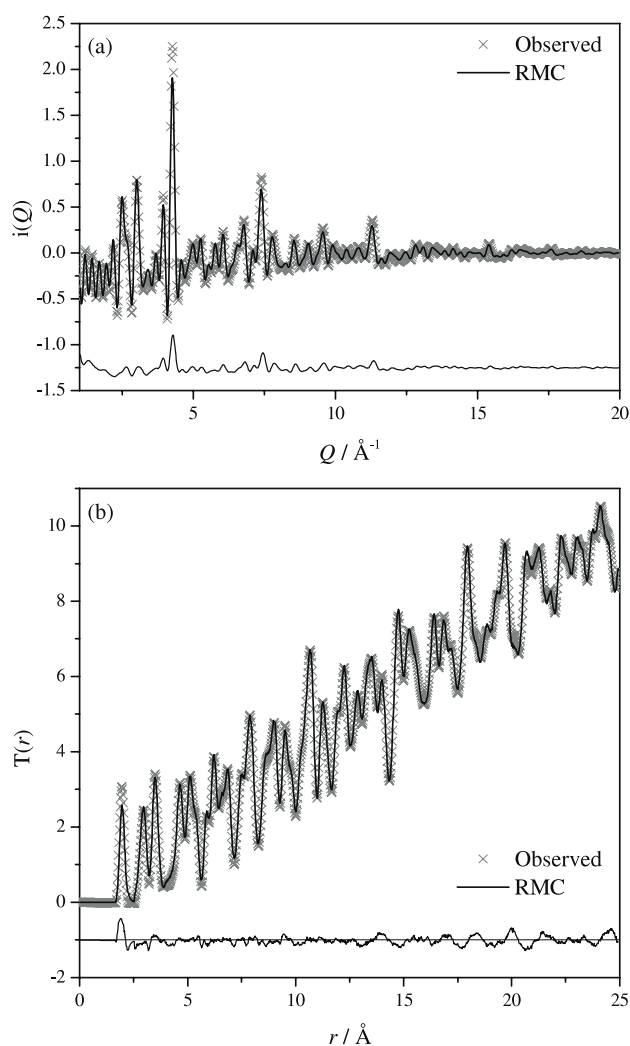
Figure 6. RMC fits to the total scattering data from the solvothermal cobalt gallate spinel. (a) The $i(Q)$ and (b) the $T(r)$.

Figure 7. The partial M–O correlation functions for the octahedral cation site. Note that the Co–O partial has been enlarged to aid visibility.

Figure 8. Zero-field-cooled warming and field-cooled cooling magnetization curves for the solvothermal cobalt gallate spinel, measured in an applied field of 100 Oe.

not deviate far from their positions in the crystallographic model. The partial correlation functions for the metal–oxygen (M–O) pairs (figure 7) imply that the CoO_6 octahedra are more distorted than the GaO_6 octahedra, as the Co–O peak is broader than the Ga–O peak. Additionally, the Ga–O peak has broadened somewhat asymmetrically from its starting point, which may be evidence of a similar 'off-centring' of the Ga atoms as was observed in γ-Ga_2O_3. The shape and position of the first PDF peak is significantly better reproduced by the refined RMC configuration than by the crystallographic model used for PDF analysis, which shows that modelling the local distortion in this material requires the symmetry constraints to be removed.

3.3. Magnetic properties

Previous reports on cobalt gallate spinels have classified them as spin glasses [29, 31], with a freezing temperature of 10 K as revealed by a divergence of the field-cooled (FC) and zero-field-cooled (ZFC) dc magnetization curves and a sharp maximum in the ac susceptibility curves at this temperature.
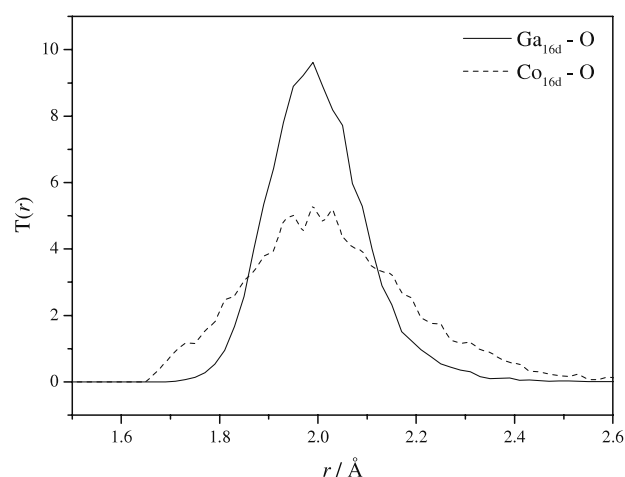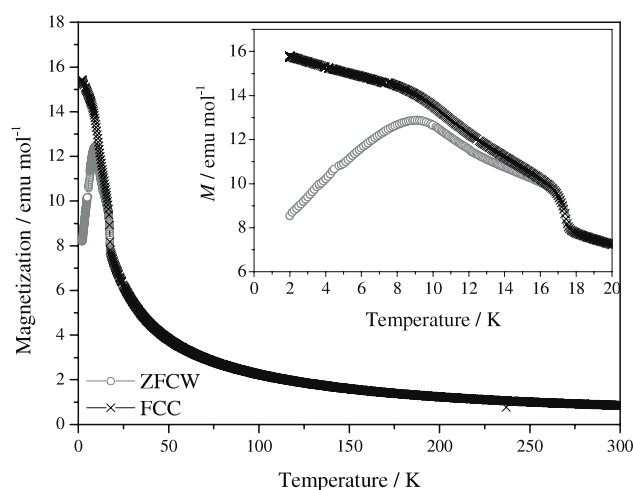
The dc magnetization curves for the solvothermal cobalt gallate are shown in figure 8, and indeed, a broad maximum is clearly visible at around 10 K. However, a small difference between the ZFC warming and FC cooling curves is observed up to around 17.5 K, and the magnetization (*M*) versus field (*H*) data (see supporting information available at stacks.iop.org/JPhysCM/25/454212/mmedia) also provide evidence that some form of magnetic ordering occurs at and below 17.5 K.

The effective magnetic moment per Co, deduced from a fit to the Curie–Weiss law of the inverse susceptibility versus temperature (supporting information available at stacks.iop.org/JPhysCM/25/454212/mmedia), is 4.76 μ_B/Co, which is in excellent agreement with the value obtained by Wakeshima *et al* for $BaLa_2CoS_5$ [50], and indicates a partial quenching of the orbital contribution to the overall magnetic moment. If the quenching were complete (as would be the case if, for example, the Jahn–Teller effect manifested in a long-range structural distortion) a value closer to the spin-only value of 3.87 μ_B/Co^{2+} would be expected. That partial quenching
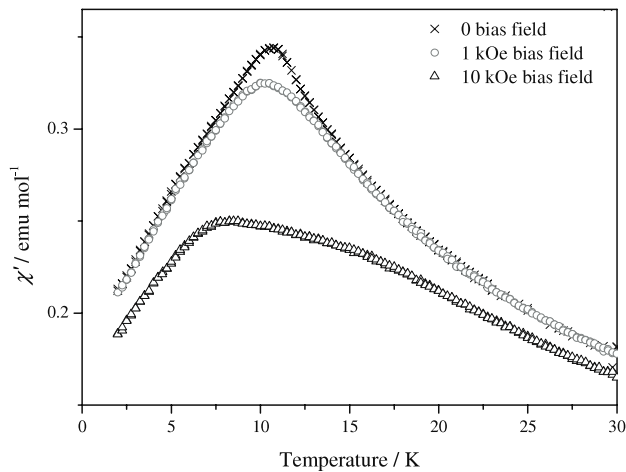
Figure 9. Temperature dependence of the real part of the ac susceptibility of the solvothermal cobalt gallate spinel in different dc bias fields. The ac measuring field was 3 Oe with a frequency of 30 Hz.

Figure 10. Temperature dependence of the real part of the ac susceptibility of the solvothermal cobalt gallate spinel at different frequencies. $H_{ac} = 3$ Oe.

is observed supports the conclusion of the total scattering experiment that a degree of local distortion around the Co^{2+} centres occurs. The Weiss temperature, θ_w, deduced from the χ^{-1} versus T plot is -21 K, indicating that the magnetic interactions are predominantly antiferromagnetic, as is expected for a spinel lattice. Additionally, $|\theta_w|$ is close to the temperature at which the first sign of magnetic order is seen in the dc magnetization.

The ac susceptibility data measured at different (dc) bias fields are shown in figure 9. A clear maximum is visible at ~ 10 K in zero bias field, which is shifted to lower temperatures as the bias field is increased. There is also a subtle change in $\chi(T)$ present at 17.5 K.

The feature in the ac susceptibility at 10 K exhibits a moderate frequency dependence (figure 10) with a shift, $\Delta T_f/[T_f \Delta(\log \omega)]$, of 0.05, somewhat larger than those usually observed for canonical spin glasses and much smaller than those for superparamagnets [51].

Isothermal magnetization measurements as a function of time at different temperatures show that there is slow evolution in the magnetic order below 10 K, while above 10 K the system evolves rapidly to reach a magnetic equilibrium (supporting information available at stacks.iop.org/JPhysCM/25/454212/mmedia). There are no features in the temperature dependence of the heat capacity that can be associated with the onset of long-range magnetic order (see figure S10 available at stacks.iop.org/JPhysCM/25/454212/mmedia).

Spinel materials with a distribution of magnetic cations across both A and B sites often exhibit ferrimagnetic ordering, as is the case for magnetite, Fe_3O_4. According to the magnetic phase diagrams determined by Poole *et al* [52], the cobalt gallate spinel is unlikely to exhibit this ordering due to the relatively low concentration of Co on both sites. In such dilute systems, spin-glass type ordering is quite common due to the combination of frustrated magnetic interactions (as each of the two cation sublattices form corner-shared tetrahedral networks) and disorder.
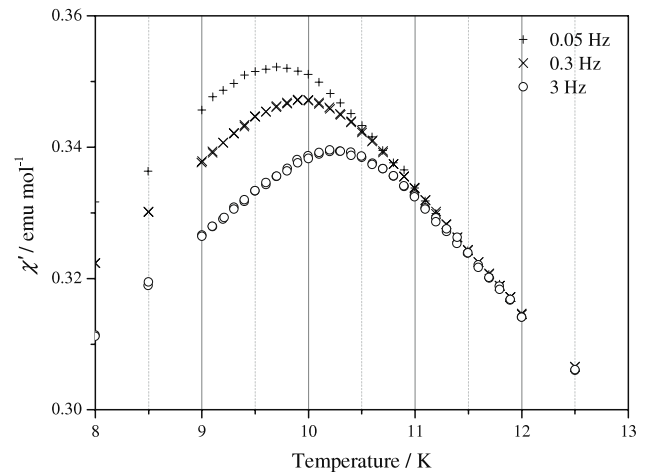
Our data suggest that short-range magnetic order develops at temperatures below 17.5 K, perhaps due to the presence of antiferromagnetically ordered clusters, and that freezing of these clusters occurs below 10 K. The presence of such clusters could potentially be confirmed using RMC refinements: a range of starting configurations with different Co/Ga distributions would be required to determine whether or not the total neutron scattering data provide evidence of clustering in the short-to-medium-range order.

4. Conclusions

The structure of a cobalt gallate material has been examined in detail, and found from Rietveld refinement to be consistent with a partially defective spinel containing mixed valent cobalt and a small number of oxygen vacancies, as well as a mixture of octahedral and tetrahedral gallium. PDF analysis using the Rietveld-derived model revealed that the model is consistent with the short-to-medium-range order in this material; however, importantly, it also revealed some discrepancies in the low-r ($r < 3.25$ Å) region. These discrepancies were found to be due to the cubic space group of the model enforcing a symmetrical octahedral environment, which we had previously found to be inappropriate for Ga^{3+}. This geometry is also likely to be disfavoured by Co^{2+} due to the Jahn–Teller effect, but is potentially appropriate for Co^{3+}, which, due to its d^6 electronic configuration is likely to be low spin and strongly favour the octahedral B site. PDF analysis has therefore revealed the complexity which arises due to the conflicting coordination preferences.

Results from RMC modelling support the conclusions from PDF analysis: that the cubic spinel structure represents the average structure extremely well but that a description of the local structure requires that the symmetry constraints be lifted. Additionally, some evidence for the octahedral cobalt environment being more distorted than the gallium environment has been obtained from the partial correlation functions of the refined RMC configuration.

Acknowledgments

References

[1] Grimes N W 1975 *Phys. Technol.* **6** 22
[2] Kawazoe H and Ueda K 1999 *J. Am. Ceram. Soc.* **82** 3330
[3] Chen Y C, Xie K, Pan Y and Zheng C M 2011 *J. Power Sources* **196** 6493
[4] Cheng F Y, Shen J A, Peng B, Pan Y D, Tao Z L and Chen J 2011 *Nature Chem.* **3** 79
[5] Wachs I E and Routray K 2012 *ACS Catal.* **2** 1235
[6] Conrad F, Bauer M, Sheptyakov D, Weyeneth S, Jaeger D, Hametner K, Car P E, Patscheider J, Gunther D and Patzke G R 2012 *RSC Adv.* **2** 3076
[7] Verwey E J W and Heilmann E L 1947 *J. Chem. Phys.* **15** 174
[8] O'Neill H St C and Navrotsky A 1983 *Am. Mineral.* **68** 181
[9] Machala L, Tuček J I and Zbořil R 2011 *Chem. Mater.* **23** 3255
[10] Smrčok L', Langer V and Křesťan J 2006 *Acta Crystallogr.* C **62** i83
[11] Berg H, Kelder E M and Thomas J O 1999 *J. Mater. Chem.* **9** 427
[12] Fleet M 1982 *Acta Crystallogr.* B **38** 1718
[13] Billinge S J L 2008 *J. Solid State Chem.* **181** 1695
[14] Young C A and Goodwin A L 2011 *J. Mater. Chem.* **21** 6464
[15] Makovec D, Kodre A, Arčon I and Drofenik M 2011 *J. Nanopart. Res.* **13** 1781
[16] Sreeja V, Smitha T S, Nand D, Ajithkumar T G and Joy P A 2008 *J. Phys. Chem.* C **112** 14737
[17] Sepelak V, Becker S M, Bergmann I, Indris S, Scheuermann M, Feldhoff A, Kubel C, Bruns M, Sturzl N, Ulrich A S, Ghafari M, Hahn H, Grey C P, Becker K D and Heitjans P 2012 *J. Mater. Chem.* **22** 3117
[18] Shoemaker D P, Li J and Seshadri R 2009 *J. Am. Chem. Soc.* **131** 11450
[19] Navrotsky A and Kleppa O J 1968 *J. Inorg. Nucl. Chem.* **30** 479
[20] Omata T, Ueda N, Hikuma N, Ueda K, Mizoguchi H, Hashimoto T and Kawazoe H 1993 *Appl. Phys. Lett.* **62** 499
[21] Omata T, Ueda N, Ueda K and Kawazoe H 1994 *Appl. Phys. Lett.* **64** 1077
[22] Liu Z S, Hu P, Jing X P and Wang L X 2009 *J. Electrochem. Soc.* **156** H43
[23] Costa G K B, Pedro S S, Carvalho I C S and Sosman L P 2009 *Opt. Mater.* **31** 1620
[24] Suzuki T, Murugan G S and Ohishi Y 2005 *J. Lumin.* **113** 265
[25] Biswas S K, Sarkar A, Pathak A and Pramanik P 2010 *Talanta* **81** 1607
[26] Chen X, Xue H, Li Z H, Wu L, Wang X X and Fu X Z 2008 *J. Phys. Chem.* C **112** 20393
[27] Gurunathan K, Baeg J O, Lee S M, Subramanian E, Moon S J and Kong K J 2008 *Int. J. Hydrog. Energy* **33** 2646
[28] Nakatsuka A, Ikeda Y, Nakayama N and Mizota T 2006 *Acta Crystallogr.* E **62** I109
[29] Soubeyroux J L, Fiorani D and Agostinelli E 1986 *J. Magn. Magn. Mater.* **54–57** 83
[30] Otero Arean C and Garcia Diaz E 1982 *Mater. Chem.* **7** 675
[31] Fiorani D and Viticoli S 1978 *Solid State Commun.* **25** 155
[32] Ahman J, Svensson G and Albertsson J 1996 *Acta Crystallogr.* C **52** 1336
[33] Feng S and Xu R 2000 *Acc. Chem. Res.* **34** 239
[34] Walton R I 2002 *Chem. Soc. Rev.* **31** 230
[35] Porta P and Anichini A 1980 *J. Chem. Soc. Faraday Trans.* I **76** 2448
[36] Sears V F 1992 *Neutron News* **3** 26
[37] Playford H Y, Hannon A C, Barney E R and Walton R I 2013 *Chem. Eur. J.* **19** 2803
[38] Arima T, Higashiyama D, Kaneko Y, He J P, Goto T, Miyasaka S, Kimura T, Oikawa K, Kamiyama T, Kumai R and Tokura Y 2004 *Phys. Rev.* B **70** 064426
[39] Hannon A C 2005 *Nucl. Instrum. Methods Phys. Res.* A **551** 88
[40] Soper A K and Buchanan P 2004 personal communication
[41] Soper A K 2011 *Rutherford Appleton Laboratory Technical Report* RAL-TR-2011–013
[42] Hannon A C, Howells W S and Soper A K 1990 *Inst. Phys. Conf. Ser.* **107** 193
[43] Lorch E 1969 *J. Phys. C: Solid State Phys.* **2** 229
[44] Larson A C and Dreele R B V 1994 *Los Alamos National Laboratory Report LAUR* 86-748
[45] Toby B H 2001 *J. Appl. Crystallogr.* **34** 210
[46] Farrow C L, Juhas P, Liu J W, Bryndin D, Božin E S, Bloch J, Proffen T and Billinge S J L 2007 *J. Phys.: Condens. Matter* **19** 335219
[47] Tucker M G, Keen D A, Dove M T, Goodwin A L and Hui Q 2007 *J. Phys.: Condens. Matter* **19** 335218
[48] Kanno R, Yonemura M, Kohigashi T, Kawamoto Y, Tabuchi M and Kamiyama T 2001 *J. Power Sources* **97/98** 423
[49] Hagen A and Östby J 2006 *Proc. 7th European Solid Oxide Fuel Cell Forum (Lucerne)* ed U Bossel (Oberrohrdorf: European Fuel Cell Forum)
[50] Wakeshima M, Hinatsu Y, Ishii Y, Shimojo Y and Morii Y 2002 *J. Mater. Chem.* **12** 631
[51] Mydosh J A 1993 *Spin Glasses An Experimental Introduction* (London: Taylor and Francis)
[52] Poole C Jr and Farach H 1982 *Z. Phys.* B **47** 55